

# PROCEEDINGS OF SPIE REPRINT



SPIE—The International Society for Optical Engineering

*Reprinted from*

## ***Lithographic and Micromachining Techniques for Optical Component Fabrication***

**29–30 July 2001  
San Diego, USA**



**Volume 4440**

©2001 by the Society of Photo-Optical Instrumentation Engineers  
P.O. Box 10, Bellingham, Washington 98227 USA. Telephone 360/676-3290.

# Quality assurance of HARMS and MOEMS surface structures using confocal white light microscopy

Hans-Joachim Jordan<sup>\*a</sup>, Rainer Brodmann<sup>\*b</sup>, Marcus Grigat<sup>\*c</sup> and Juergen Valentin<sup>\*d</sup>  
NanoFocus Messtechnik GmbH, Duisburg, Germany

## ABSTRACT

The commercial success in micro-system technologies depends on a reliable and controlled mass production. Without a good quality assurance and process control it is impossible to guarantee the specifications of the products and to minimize the production costs. Among test equipment for the function of the end product it is necessary to introduce dimensional metrology devices for checking vertical and lateral structures in silicon or PMMA materials close to production machines. Due to the small dimensions of HARMS or MOEMS components, traditional surface testers as mechanical stylus instruments are not able to analyse structures with high aspect ratio. In this paper a new approach to surface measurement technique, the confocal white light microscopy, is described which opens the possibility to measure soft or transparent materials from the nanometer up to the millimetre range. In contrast to other methods, like phase shift interferometry, the confocal measurement technique is nearly free of artefacts due to physical pinhole filter masks.

Keywords: 3D confocal microscopy, non-contact 3D characterization, 3D topographic analysis, master – replication comparison, automated 3D measuring system

## 1. INTRODUCTION

Confocal microscopy, as first described by M. Minsky<sup>1,2</sup> in 1957 and originally named “double focusing microscopy” becomes a more and more powerful tool for accurate 3D characterisation of rough, complex or micro-structured surfaces.

In the reflection mode *1D confocal point distance measurement*, light emitted from a point light source is imaged into the object focal plane of a microscope objective (the first focussing). A in-focus specimen location results in a maximum flux of the reflected light through a detector pinhole (the second focussing), whereas light from defocused object regions is partly suppressed (Figure 1). Thus, the detector signal as limited by the pinhole size is reduced strongly when defocusing the specimen, which allows the *1D confocal point distance measurement* by the so called depth discrimination<sup>3,4</sup>.

Different designs of *3D confocal microscopes* are possible for the acquisition and evaluation of topographic data. Time consuming serial *xy*-scanning techniques on the basis of the *1D confocal point distance measurement* have been developed for the acquisition of depth discriminated sections in confocal laser scanning microscopes and a further *z*-scan is still necessary to acquire all the data for the evaluation of 3D topographic maps<sup>5,6</sup>.

For *xy*-scanning, the NanoFocus<sup>TM</sup>  $\mu$ Surf<sup>TM</sup> *3D confocal microscope* is using a multiple pinhole mask (Nipkow disk) in an intermediate image plane of a microscope as first described by Petran<sup>7</sup>. Combined with CCD image processing, the rotating Nipkow disk affects the *xy*-scan of the object field in video-real-time. Just an additional *z*-scan is necessary for 3D acquisition<sup>8,9</sup>.

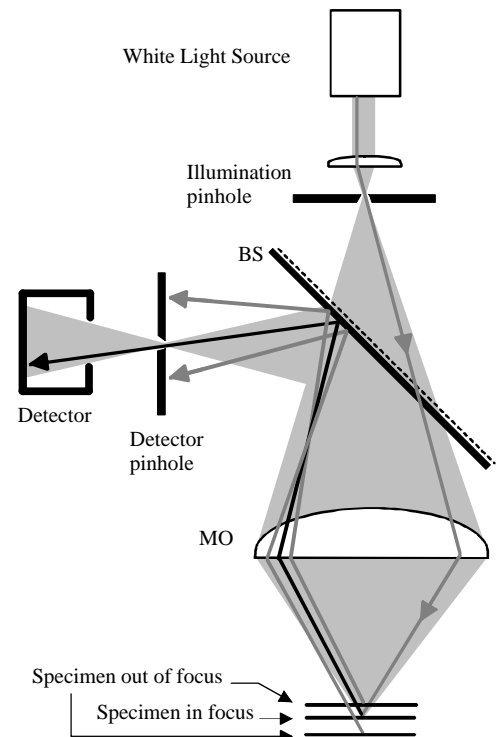


Figure 1: The basic principle of the *1D confocal point distance measurement*.

\*a jordan-consulting@gmx.de; \*b brodmann@nanofocus.de; \*c grigat@nanofocus.de; \*d valentin@nanofocus.de;  
\*a - \*d phone +49.203.306.1880; fax +49.203.306.1899; NanoFocus Messtechnik GmbH, Bismarckstrasse 120, Duisburg, D 47057, Germany

The Nipkow-disk expands the effect of depth discrimination to the area of the microscope object field, which allows optical sectioning like in computer tomography. Two additional improvements of *3D confocal microscopy* against other types of classical 3D microscopes are first the contrast enhancement by suppression of light scattered from defocused specimen locations and second an increase of the lateral resolution of about 20%<sup>10</sup>.

## 2. A SHORT THEORY OF 3D CONFOCAL MICROSCOPY

A comprehensive description of the theory of confocal microscopy is given by Wilson<sup>10</sup>, relevant formulas for 3D topometry are as follows<sup>8,9,11</sup>.

The depth response  $I(z)$  of a confocal system is proportional to a  $SINC^2$  function,

$$I(z) = \left( \frac{\sin(kz(1 - \cos \mathbf{a}))}{kz(1 - \cos \mathbf{a})} \right)^2 I_0 \quad (1)$$

which is depending on the aperture angle  $\mathbf{a}$  of the microscope objective, the wavelength of light  $I$ , the wavenumber  $k = 2\pi/I$  and the co-ordinate of defocusing  $z$ .

Significant for the depth response  $I(z)$  is the Full Width at Half Maximum, which is

$$FWHM = 2z_{1/2} \approx \frac{0,443I}{1 - \cos \mathbf{a}} \quad (2)$$

The half angle of the numerical aperture  $NA$  determines the maximum surface slope

$$\mathbf{a}_{\max}^{spec} = 0.5 \sin^{-1} NA \quad (3)$$

for specular reflection at a microscopic smooth surface element of the specimen. The wavelength together with the numerical aperture determine the full width at half maximum  $FWHM$  of the depth response  $I(z)$  of the detectors intensity.

Engineering surfaces often have micro-roughness within the probe spot size, therefore diffuse reflection increases the maximum surface slope which can be measured ( $\mathbf{a}^{diff} \geq \mathbf{a}_{\max}^{spec}$ ) and  $\mathbf{a}_{\max}^{spec}$  according to equation 3 indicates a lower limit of the surface slope.

## 3. THE NANOFOCUS™ μSURF™ 3D CONFOCAL MICROSCOPE

For  $xy$ -scanning of a depth discriminated section we use a spinning Nipkow-disk, which consists of an array of pinholes arranged in a spiral shape. The spinning disk is illuminated by a plane wave and acts as a scanning multiple point light source, which is imaged into the object focal plane of the microscope objective. After the reflection of light, each illuminating Nipkow pinhole acts as his own detector pinhole (figure 3). The depth discriminated  $xy$  information  $I(x,y,z)$  is imaged onto a CCD camera. Thus, during one rotation of the disk, a  $xy$ -section of the specimen of constant height is acquired in video real-time. Image processing and height evaluation is done using a  $512 \times 512$  pixel frame-grabber.

By an additional  $z$ -scan of the specimen, a stack  $z_1$  to  $z_n$  ( $n < 3000$ ) of depth discriminated CCD camera-frames is acquired, from which a 3D topography can be constructed with an resolution of about 1% of the FWHM. In figure 4, a measured depth response  $I(x_i, y_j, z)$  and the mode of evaluation of the height coordinate  $h(x_i, y_j)$  as the centre of  $I(x_i, y_j, z)$  is presented. A well formed depth response according to the equations 1 and 2 is decisive for accurate *3D confocal microscopy*.

The μSurf™ measurement station (figure 5) consists of a compact confocal module, which includes all the optics. An external Xenon lamp is connected to the confocal module via a light guide. The confocal module is fixed on the precise stepper motor driven linear axis which is mounted on a solid bridge stand. The sample is placed on an  $xy$  precision slide and the confocal module is moved stepwise in  $z$ -direction (Piezo with up to 350μm travel and 10nm resolution or precise stepper motor driven linear axis with 100mm travel and 100nm resolution). The NanoFocus™ μSurf™ confocal microscope is controlled by software running under Microsoft™ Windows™ (95 / 98 / NT4.0 / 2000). The surface topographic data can be visualised and analysed in various ways. Technical data of the μSurf™ are summarised in Table 1.

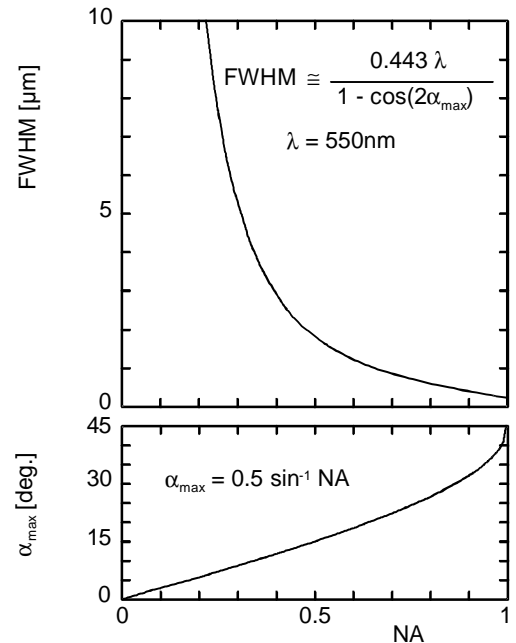


**Figure 2:** Graphs of the full width of half maximum of the confocal depth response (equation (2)) and of the maximum surface slope for specular reflection (equation (3)) versus the numerical aperture.

The accuracy of the  $\mu\text{Surf}^{\text{TM}}$  measurement principle have been approved in all 3 co-ordinates using several standards like the PTB depth setting or the PTB roughness standards <sup>8, 9</sup>. In former comparisons to tactile instruments a very good agreement not only in the profile records but also in roughness parameters was obtained <sup>8,9</sup>.

Based on the high accuracy of the  $\mu\text{Surf}^{\text{TM}}$  topographic data, a very powerful and effective stitching has been developed in order to overcome the limitation of the microscopes object field size without loss of lateral resolution. For stitching, a set of single object field topographies were acquired with an field overlap between neighboured measurements of about 10% of the single measurement field size. After the acquisition of all single object field topographies, neighboured single object field topographies were combined using a correlation algorithm, which works in all 3 axis.

The principle of stitching is demonstrated in figure 6, with a LASERTEX sheet as an example. This specimen shows roughness as well as a complex form. Although this specimen has very steep slopes (up to 65 degrees), the back-scattered light - due to the micro-roughness of highest spatial frequencies - was sufficient for accurate single field measurements. After the procedure as demonstrated in figure 6, the elimination of vertical offsets is done using a height correlation in order to obtain the final result.

It should be noticed that all presentations within this paper are showing raw data of the  $\mu\text{Surf}^{\text{TM}}$  system. No artefacts or spikes have been filtered out in any plot.

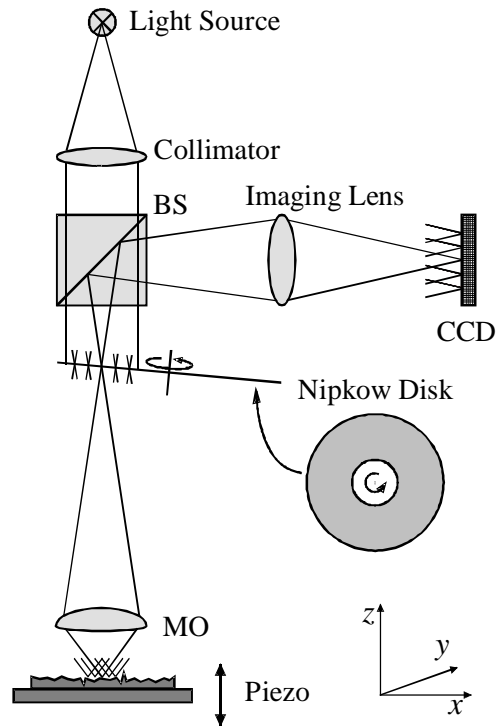


**Figure 3:** The  $\mu\text{Surf}^{\text{TM}}$  set-up, using a spinning Nipkow-disk

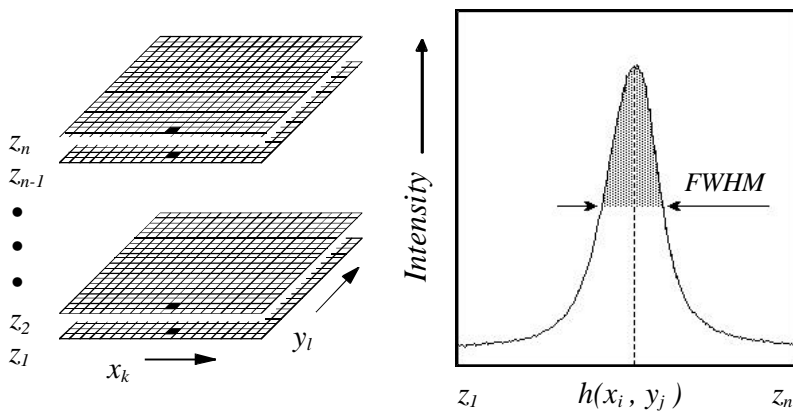


**Figure 4:** The evaluation of the topography: Calculation of the height coordinate  $h(x_i, y_j)$  as the centre of the depth response  $I(x_i, y_j, z)$  for each pixel of the stack  $z_1$  to  $z_n$ .



**Figure 5:** The  $\mu\text{Surf}^{\text{TM}}$  measurement station

Microscope objective	10×	20×	50×	100×
Typical single object field size [ $\mu\text{m} \times \mu\text{m}$ ]	1600 × 1510	800 × 755	320 × 302	160 × 151
Working distance [mm]	10,1	3,1 / 12,0*	0,66 / 10,6*	0,31 / 3,4*
Numerical aperture	0,30	0,46 / 0,40*	0,80 / 0,50*	0,95 / 0,80*
Maximum. slope for specular reflection [deg.]	8,7	13,7 / 11,7*	26,6 / 15,0*	35,9 / 26,6*
Vertical resolution [nm]	50	<30 / <20**	<20 / <10**	<20 / <5**

**Table 1:** Technical data of the  $\mu\text{Surf}^{\text{TM}}$  (\* Long working distance / \*\* Piezo for high resolution).

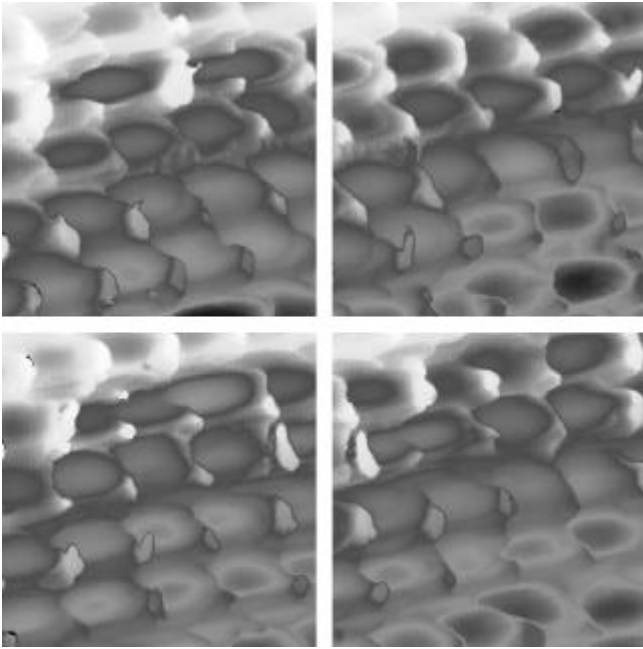
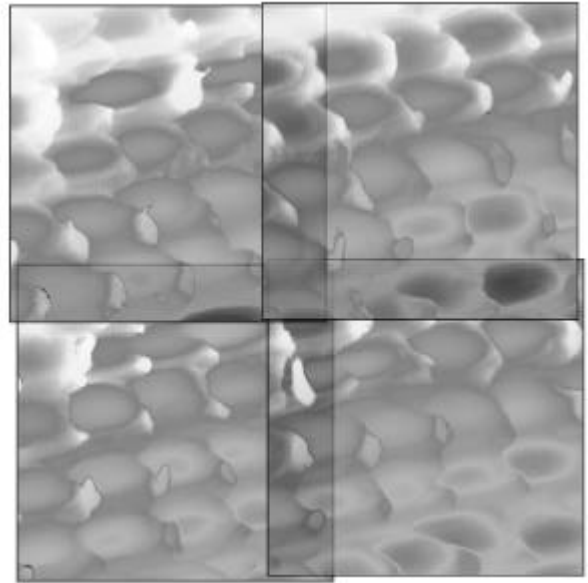


**Figure 6:** An example of a 2×2 μSurf™ stitching.

*Left:* 4 single measurements, each with an overlap of about 10% to the neighbored one.



*Right:* In a first step, a stitching of patterns eliminates all possible positioning errors of the *xy*-stages. In a second step, a height correlation of the overlapping areas eliminates offset inaccuracies of the *z*-stage.

#### 4. MASTER – REPLICATION COMPARISON

The first μSurf™ application shows the comparison of a refractive spherical micro-lens-array master and its hot embossed replication. This work was part of the BMBF-project *NanoFab*, funded by the German government.

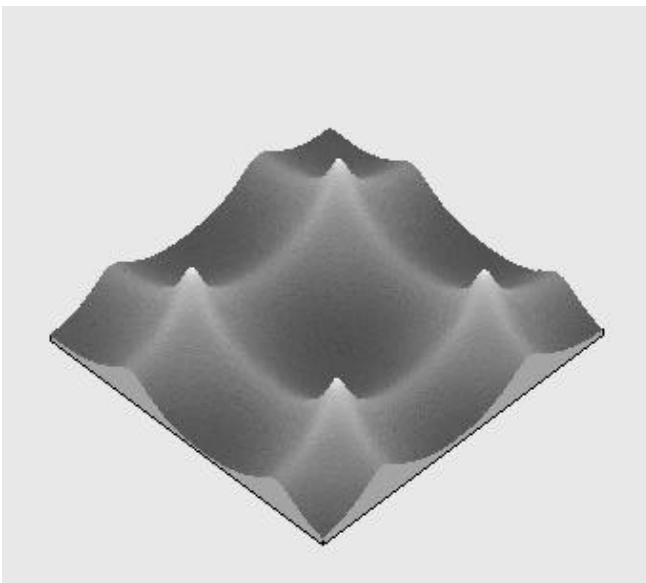


**Figure 7:** 3D topography of a refractive micro-lens-array master, measured with the μSurf.

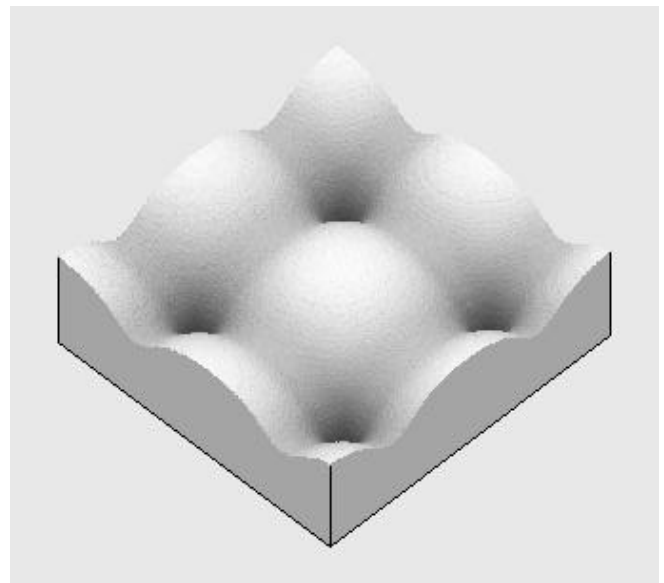


**Figure 8:** 3D topography of a hot-embossed replication of the refractive micro-lens-array master (μSurf measurement).

The aim of the *NanoFab* project is the development of a process chain for the mass reproduction of 3D micro- and nano-structures on ‘large areas’ for various applications like self-adhesive foils with properties like antireflection-coatings, self-cleaning by Lotus-effect or the reduction of air-resistance by the shark-skin effect.

Beginning from a 1<sup>st</sup> order master of a micro- and nano-structure with a corresponding area of less than 1mm<sup>2</sup>, a 2<sup>nd</sup> order master should be produced by step-and-repeat processes with a corresponding reproduction area in the size of square-centimeters, quite similar to the  $\mu\text{Surf}^{\text{TM}}$  stitching procedure. Doing the same with the 2<sup>nd</sup> order master results in a 3<sup>rd</sup> order master of the size of square-decimeters, and so on. It is evident that the quality of the end product is significantly depending on the reproduction quality of each single step and the power of reproductions.

Figure 7 shows the 3D topography of a refractive spherical micro-lens-array master and figure 8 the 3D topography of a hot-embossed replication, both from  $\mu\text{Surf}^{\text{TM}}$  measurements. This measurements have been carried out using a 50 $\times$  microscope objective with long working distance of 10.6 mm. The measured object field size for both topographies is about (280  $\mu\text{m}$ )<sup>2</sup> and the measured topography peak-to-valley is about 7.5  $\mu\text{m}$ .

The nominal micro-lens radius of curvature for this example is 1mm. The question are ‘What is the radius accuracy?’ and ‘How do master and hot-embossed reproduction compare?’, that means ‘What is the quality of reproduction?’.

Figure 9 shows the same 3D topography as figure 8, together with the orientation of 2 profiles P1 and P2 as significant cross-sections of the 3D topography.

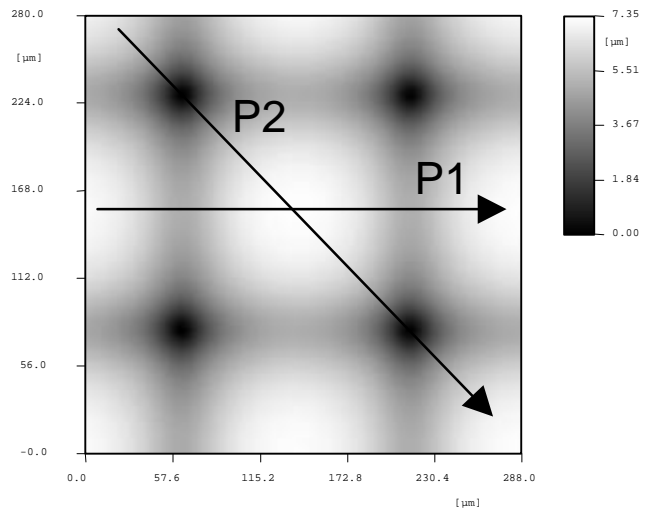
Figure 10 shows the parallel profile P1 from the left to the right center of the borderlines between neighbored square-sized micro-lenses, crossing the center of the lens. Here we have a good agreement of the profile P1 and the 1mm sphere radius all over the cross-section.

Figure 11 shows the diagonal profile P2 between two diagonal corners of the square-sized micro-lenses, also crossing the center of the lens. A difference of up to 2 microns compared to the 1mm sphere radius appears in the corners of the lenses.

Those properties of form correspondence (figure 10) and form deviation (figure 11) are quite similar also for the topography of the master from figure 7, not only for the topography of the replication (figure 8).

Up to now we have some information on form deviations from the sphere for the master as well as for the replication, but not on the quality of reproduction itself.

To look on this, the 3D topography of the replication from figure 8 has to be inverted in the z co-ordinate and mirrored in the x co-ordinate in order to be subtracted from the 3D topography of the master from figure 7. Doing this and eliminating lateral displacements between both data sets by correlation methods before the subtraction results in the 3D difference as shown in figure 12.



**Figure 9:** Top of view presentation of the topography from figure 8, showing the orientation of profiles P1 and P2.

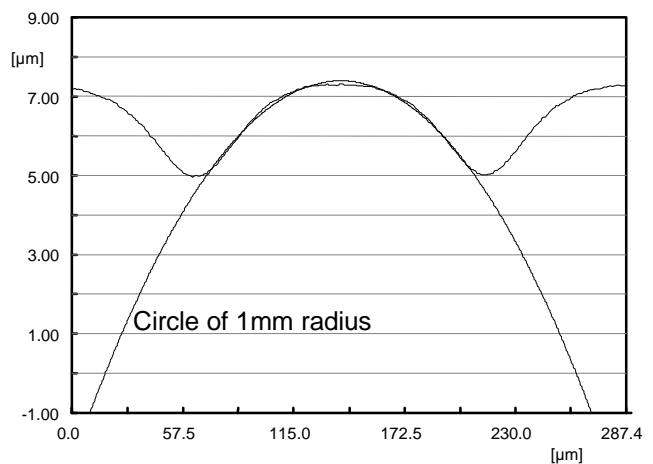


**Figure 10:** Cross-section of the topography from figure 8 due to the parallel profile P1 and a radius of 1mm.

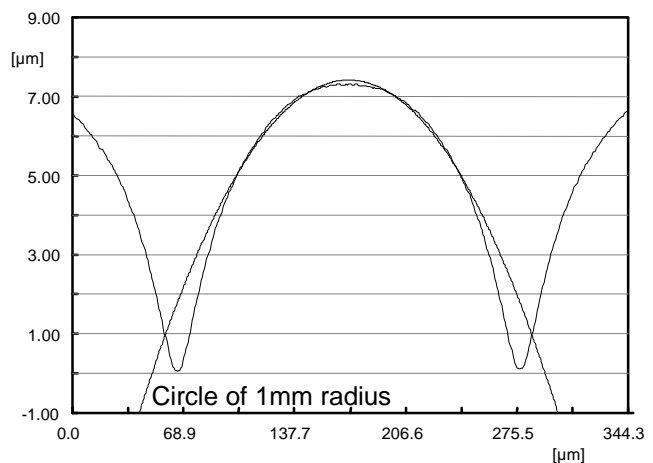


**Figure 11:** Cross-section of the topography from figure 8 due to the diagonal profile P2 and a radius of 1mm.

The 3D difference of both topographies looks flat within the center area of each micro-lens. Some walls appear along the border lines between two neighbored micro-lenses and some 'strong' peaks in the corners where four micro-lenses meet. Corresponding to figure 10, figure 13 shows the parallel difference profile P1 from the left to the right center of the borderlines between neighbored square-sized micro-lenses, crossing the center of the lens. In the center of a micro-lens, the difference between the master and its replication is flat down to deviations of below 100 nanometers. At the borderlines between two neighbored square-sized micro-lenses a difference of about 200 nanometers appears between the master and its replication.

Corresponding to figure 11, figure 14 shows the diagonal difference profile P2 between two diagonal corners of the square-sized micro-lenses, also crossing the center of the lens. In the corners, where four square-sized micro-lenses meet, a difference of about 500 nanometers appears between the master and its replication.

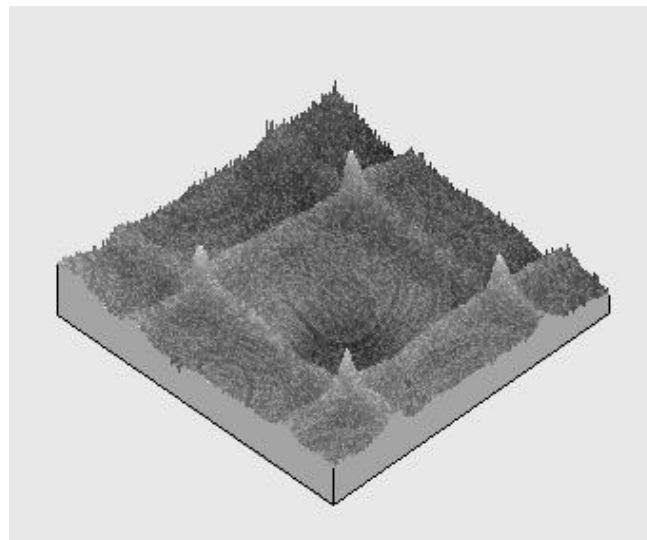


**Figure 12:** 3D difference of the topography from figure 7 (master) and the z-inverted, x-mirrored and lateral correlated topography from figure 8 (replication).

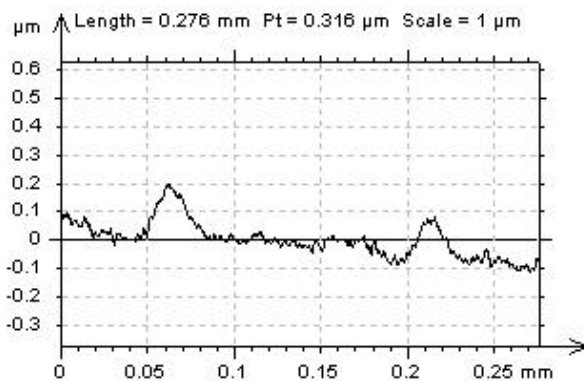


**Figure 13:** Cross-section of the 3D difference from figure 12 due to the orientation of the parallel profile P1, see figure 9.

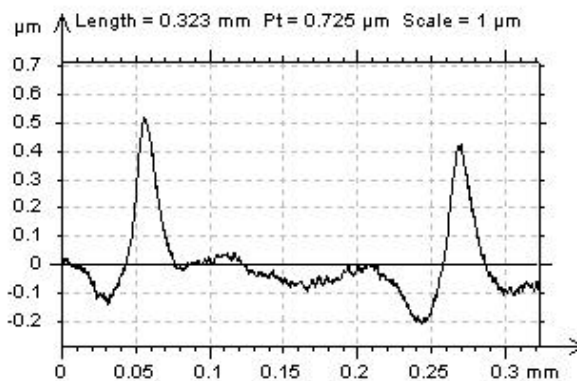


**Figure 14:** Cross-section of the 3D difference from figure 12 due to the orientation of the diagonal profile P2, see figure 9.

## 5. AUTOMATED QUALITY CONTROL OF MEMS

NanoFocus has developed an automated confocal measuring system (*μsurf PRO*, figure 15), which fulfills the industrial demands for the quality assurance control for a series production of MEMS like for example micro-fluidic structures (figure 16). The device is embedded into the process chain of a cluster tool and is controlled by a central control unit within the local area network (LAN) of the cluster. All important opto-mechanical parts of the system (objectives, illumination, Nipkow-disk) are computer-controlled and can be adapted to the special demands of the measurement process. The measurement procedure itself is subdivided into two steps: In a first step the wafer-shaped samples are checked on irregularities in the classical microscope (vision) mode. In a second step, the locations which have been marked as "critical" before, are measured in the confocal (measuring) mode. A pick-and-place robot cares for the upload and download of the samples. The file-based measurement parameters are transmitted to the system by the cluster tool control unit. All input and output is based on the international XML-Standard to ensure simplicity of data processing and flexibility for the future. The measurement sample is for example a replicated polymer micro-fluidic structure for biomedical and pharmaceutical applications. The topography from figure 16 was obtained using the *μSurf™ PRO* with a 10× microscope objective, a working distance of 10.1 mm, a single object field size of 1440 μm × 1400 μm and a 2×2 stitching.



**Figure 15:** Automated confocal microscope ( $\mu$ surf PRO)

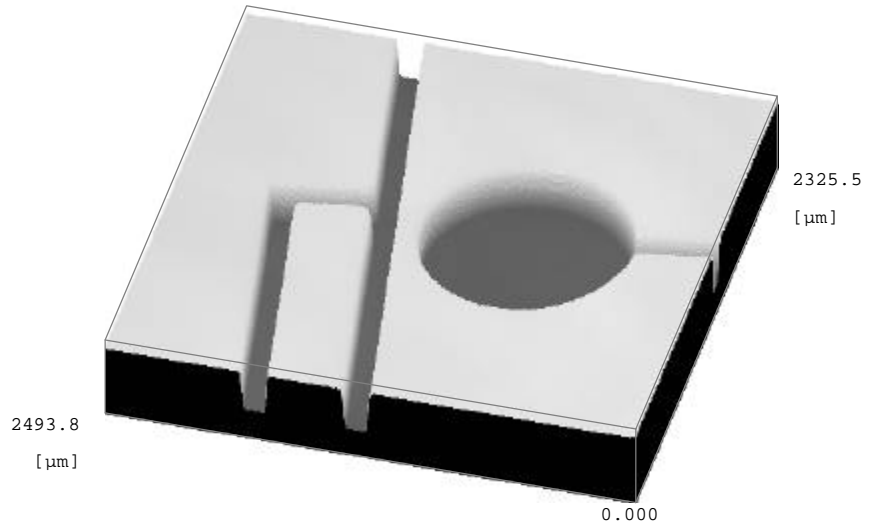


**Figure 16:** Measured micro-fluidic structure (PMMA)

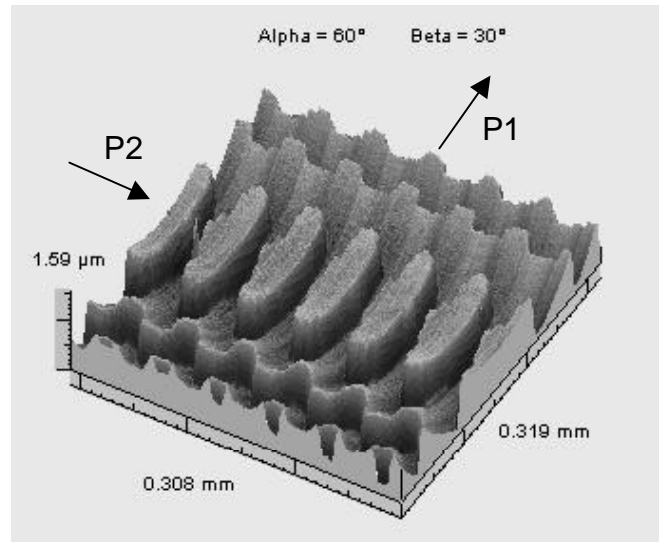
The depth of the micro-fluidic channels from figure 16 is about  $30\mu\text{m}$  at a width of about  $120\mu\text{m}$ . The edges of the micro-fluidic channels which have been measured in the topography from figure 16 are very steep, in practice they are 90 degrees. The measurement of the micro-fluidic channels is nearly free of artifacts, in practice artifacts are neglectable. The automated quality control of the  $\mu$ surf PRO is a state-of-the-art-solution for MEMs quality control. It allows a fast detection of product faults and helps to optimize the process parameters without interrupting the process.

## 6. COMPLEX SURFACE ANALYSIS

The next  $\mu$ Surf<sup>TM</sup> application shows a diffractive cylinder-micro-lens as an example for a complex surface, which both shows form as well as high spatial frequencies.

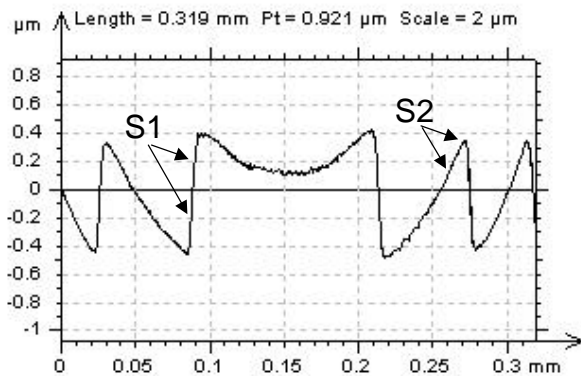
The 3D topography from figure 17 has been measured using the  $50\times$  microscope objective with long working distance of  $10.6\text{ mm}$  ( $\text{NA} = 0.5$ ). The object field size was  $320\text{ }\mu\text{m} \times 308\text{ }\mu\text{m}$  and the measured topography peak-to-valley height is only  $1.6\text{ }\mu\text{m}$ .

Figure 17 also shows the orientation of the profiles P1 from figure 18 and P2 from figure 19. Both profiles show perpendicular cross-sections through the center of the topography. Although the small topography peak-to-valley height, the surface slopes are partly not so easy to measure. The flank S1 in profile P1 (figure 18) has a slope of about 15 degrees, S2 (also figure 18) has only 1.5 degrees. In the orthogonal direction, S3 in profile P2 (figure 19) has about 20 degrees, which is above the angle  $\alpha_{\text{max}}^{\text{spec}}$  for the  $50\times$  microscope objective with long working distance (see table 1 and also figure 2). For many other types of optical 3D techniques surface slopes of this order become critical and cause artifacts in the 3D topographies. The  $\mu$ Surf<sup>TM</sup> set-up



**Figure 17:** 3D topography of a diffractive cylinder micro-lens, measured with the  $\mu$ Surf.

avoids such artifacts due to the physical pinhole filter masks, which guarantees the strong optical conjugation between the object volume and the image plane at the CCD detector.



**Figure 18:** Cross-section of the topography from figure 17 due to the direction of profile P1.

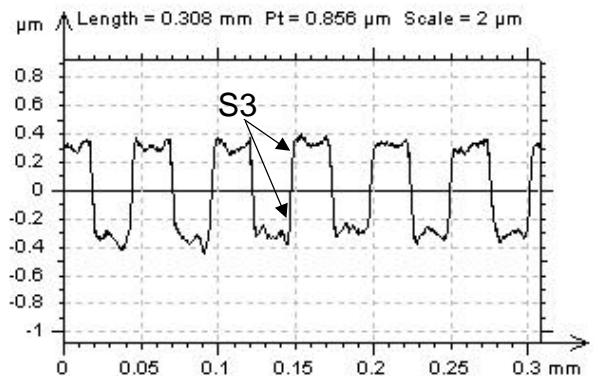


**Figure 19:** Cross-section of the topography from figure 17 due to the direction of profile P2.

## 7. CONCLUSIONS

The NanoFocus™  $\mu$ Surf™ is a powerful instrument for fast and accurate non-contact 3D surface topography measurements, comparable to tactile instruments. Furthermore, this technique gives access to measurements on steep slopes and high aspect ratios. Using the stitching tool large object fields become possible. Thus, for laboratory applications, the  $\mu$ Surf™ is an powerful alternative to tactile instruments. The  $\mu$ Surf™ PRO allows quality assurance control for MEMs series production. The images in figures 6, 9, 10, 11 and 16 have been produced using the  $\mu$ surf Software from NanoFocus. The images in figures 7, 8, 12-14 and 17-19 have been produced using the MountainsMap™ software from Digital Surf™.

## 8. ACKNOWLEDGEMENTS

The authors gratefully acknowledge the *Bundesministerium für Bildung und Forschung* for their financial support to the *NanoFab* project (“Herstellung und Replikation von großflächigen 3D Nano- und Mikrostrukturen”).

## References

1. Minsky M., Microscopy Apparatus, U.S. Patent 3013467 (19 Dec. 1961, filed 7 November 1957)
2. Minsky M., “Memoir on Inventing the Confocal Scanning Microscope”, *Scanning* **10(4)**, 128-138, 1988
3. Hamilton D. K., Wilson T., and Sheppard C. J. R., “Experimental observation of the depth-discrimination properties of scanning microscopes”, *Opt. Lett.* **6 No 12**, 625, 1981
4. Wilson T., “Depth response of scanning microscopes”, *Optik* **81 No 3**, 113, 1989
5. Hamilton D. K. and Wilson T., “Three-dimensional Surface Measurement using the confocal scanning microscope”, *Appl. Phys.* **B 27**, 211, 1982
6. Carlsson K. and Åslund N., “Confocal imaging for 3-D digital microscopy”, *Appl. Opt.* **26 No 16**, 3232, 1987
7. Petran M., Hadravsky M., Egger M. D. and Galambos R., “Tandem-Scanning Reflected-Light Microscope”, *J. Opt. Soc. Am.* **58(5)**, 661, 1968
8. Jordan H.-J., Wegner M., and Tiziani H., “Optical topometry for roughness measurement and form analysis of engineering surfaces using confocal microscopy”, *Progress in Precision Engineering and Nanotechnology*, Kunzmann H., Wäldele F., Wilkening G., Corbett J., McKeown P., Weck M., Hümmeler J. (Eds.), Vol.1, 171-174, Physikalisch-Technische Bundesanstalt Braunschweig und Berlin, Braunschweig / Germany, 1997
9. Jordan H.-J., Wegner M., and Tiziani H., “Highly accurate non-contact characterisation of engineering surfaces using confocal microscopy”, *Meas. Sci. Technol.* **9**, 1142-1151, 1998
10. Wilson T., *Confocal Microscopy*, Academic Press, 1990
11. Jordan H.-J., Brodmann R., “Highly accurate surface measurements by means of white light confocal microscopy”, X. *International Colloquium on Surfaces*, Dietzsch M., Trumbold H. (Eds.), 296-301, Shaker Verlag, Aachen, 2000